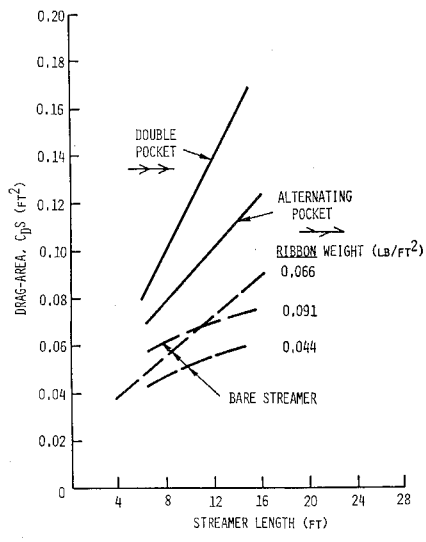

Fig. 3 Comparison of bare, alternating pocket, and double pocket-streamer drag area with length.

Results

Comparative drag coefficients for the various decelerators tested are listed in Table 1. These data were taken at a speed of 200 fps. Data taken at 100, 150, and 300 fps gave almost identical drag coefficients, as would be expected. The slotted solid parachutes had the highest drag coefficient of 0.69 but showed the usual instability of a solid chute (15°–20° oscillation).

The guide surface parachutes gave an average drag coefficient of 0.6, and they were stable with no oscillation. The less porous ring-slot parachutes had an average drag coefficient of 0.5; and the more porous, 0.36. All ring-slot chutes had a high rate of rotation, necessitating the use of a swivel, as did the cross chutes. No drag measurements could be obtained on the cross-type because they rolled up. The ring-slot chutes exhibited canopy closure at the highest velocity of 300 fps.

Figure 3 shows the variation of flat, alternating pocket, and double pocket 2-in.-wide streamer drag area as a function of streamer length. The flat 2-in.-wide, 15-ft-long ribbon streamer produced a drag coefficient of 0.084, based on 1 ft² reference area. The addition of double-opposed pockets every foot, as shown in Fig. 2, raised the drag coefficient to 0.164, or 95% more than without the pockets. This configuration was chosen for the initial stabilization of the unstable shape. A 1-ft-diam guide surface parachute was chosen as the final decelerator stage because of its excellent stability and high-drag coefficient.

Table 1 Summary of decelerator tests in low-speed wind tunnel

Decelerator type	Model number	D Constructed diameter (in.)	C_D[a]
Guide surface	P_1	12	0.55
	P_2	18	0.65
	P_3	24	0.58
	P_4	12	0.64
Slotted solid	P_5	15	0.69
	P_6	18	0.69
Ring slot	P_7	9	0.36
(more porous)	P_8	12	0.28
	P_9	15	0.36
	P_{10}	18	0.41
Ring slot	P_{11}	12	0.53
(less porous)	P_{12}	15	0.47
	P_{13}	18	0.50
Streamer		Length	
	S_1	15 ft	0.084 (flat 2-in.-wide ribbon)
	S_2	15.75 ft	0.164 (double pockets)

[a] C_D for items P_1 through P_{13} are based on constructed area $(\pi/4)D^2$; and for the streamers S_1 and S_2, the reference area is 1 ft².

Conclusions

From low-speed wind-tunnel tests of small guide surface, slotted solid, ring-slot, cross, and streamer decelerators, the following conclusions can be made: 1) The guide surface canopy design was most favorable, having a high-drag efficiency (C_D = 0.6) and excellent stability for all sizes tested from 1 to 2-ft diam; and 2) The new alternating pocket streamer design is a cheap, reliable method of providing a small drag increment for initial body stabilization.

Reference

[1] Holbrook, J. W., "Low Speed Wind Tunnel Handbook," LTV Publication AER-AOR-12995-B, May 1968, LTV Aerospace Corp.

Measurements of Particulated Gas Flow Pressure on Cascade Nozzles

W. Tabakoff* and M. F. Hussein†
University of Cincinnati, Cincinnati, Ohio

Cascade Tunnel and Model Description

A SPECIAL subsonic cascade tunnel was built which incorporates a device for injection of solid particles (Fig. 1). The cascade dimensions and the pressure probe locations are shown in Fig. 2. Further test facility information may be obtained from Ref. 1.

Instrumentation

Manometer readings were recorded by camera after a steady state was reached. The primary mass flow was measured by an orifice meter located ahead of the settling chamber. The primary flow temperature was measured with a standard thermocouple located in the settling chamber. An electronic counter was employed to record the time of par-

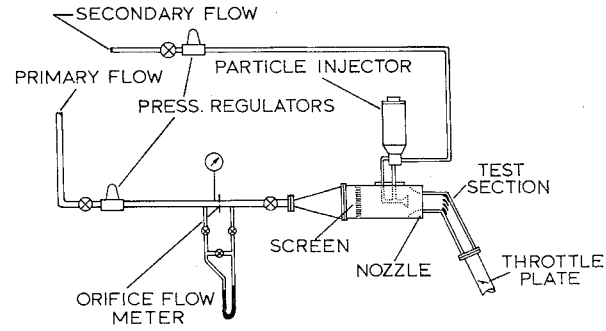

Fig. 1 Cascade tunnel schematic.

Presented as Paper 70-712 at the AIAA 6th Propulsion Joint Specialist Conference, San Diego, Calif., June 15–19, 1970; submitted July 13, 1970; revision received October 13, 1970. This work was sponsored under Project Themis Contract No. DAHC-04-69C-0016, U.S. Army Research Office—Durham.

* Professor, Department of Aerospace Engineering. Associate Fellow AIAA.

† Graduate Research Assistant, Department of Aerospace Engineering. Student Member AIAA.

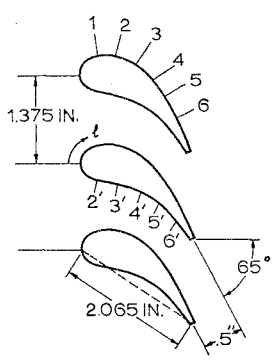

SUCTION SIDE	
1	ℓ = 0.400 IN.
2	0.690
3	1.065
4	1.425
5	1.750
6	2.140

PRESSURE SIDE	
1'	ℓ = 0.000 IN.
2'	0.437
3'	0.812
4'	1.187
5'	1.499
6'	1.903

Fig. 2 Cascade dimensions and pressure probe locations on airfoil.

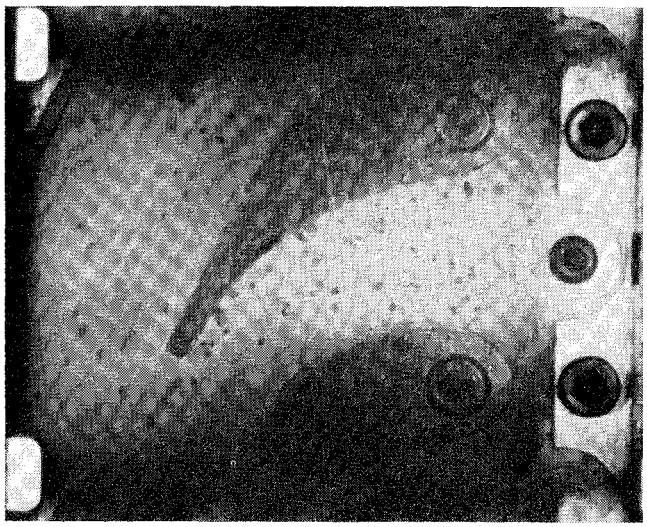

Fig. 3 High-speed photograph of particles in cascade tunnel.

ticle injection. Solid particle velocities were determined by high-speed photographing of particle trajectories. A satisfactory particle distribution is illustrated in the film frame shown in Fig. 3.

Test Conditions and Procedures

The concentration factor α is defined as $\alpha = W_p/(W_p + W_a)$ where W_p = rate mass flow of particles lb/sec and W_a = rate of air mass flow lb/sec. The cascade inlet conditions (inlet Mach number, pressure and mass flow) were calculated from the experimental data. The pressure distribution on the blade surface was evaluated for both pressure and suctions sides and plotted vs the distance (l) along the blade surface

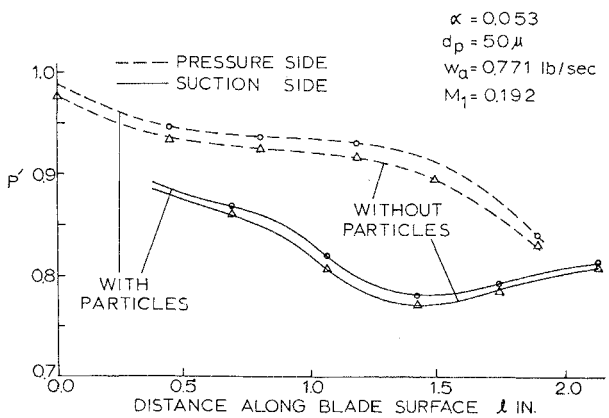

Fig. 4 Nondimensional pressure distribution on blade.

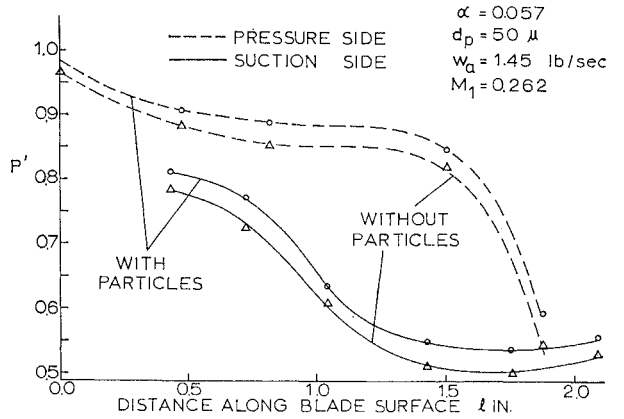

Fig. 5 Nondimensional pressure distribution on blade.

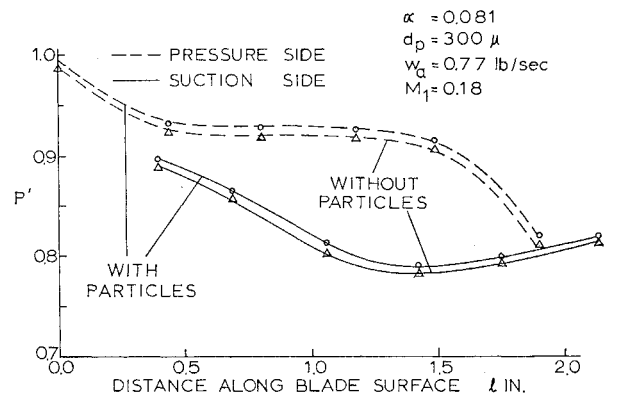

Fig. 6 Nondimensional pressure distribution on blade.

from the leading edge point. Data were obtained for mass flow from 0.70 to 1.50 lb/sec with velocities corresponding to inlet Mach numbers ranging from 0.18 to 0.275 and concentrations (α) from 0.020 to 0.085. Three different kinds of particles were used in this investigation. Table 1 shows the properties of these particles.

The inlet conditions of the gas flow were controlled by regulating valves and the mass flow metered by a flow meter. Before data could be taken, the flow had to reach steady state which was reached in a relatively short time. The pressure measurements, on the test model, were taken first without solid particles. A second group of measurements was taken with the incorporation of solid particles in the flow. The mass flow of the particles was metered and adjusted to obtain the desired concentration.

A main difficulty in recording the pressure distributions on the blades was pressure port blockage by the particles injected into the flow, especially at points on the pressure side near the leading edge. The pressure probes had to be cleaned after each run to minimize the number of blocked ports.

The uniformity of particle distribution depends on the location of the particle injector, the particle size, the density, the shape, and the tunnel pressure. Several trials were made and different injection nozzles were used until a satisfactory uniform particle distribution was obtained.

Table 1 Solid particles characteristics

Particle		Particle material density $\bar{\rho}_p$, gr/cm³	Average particle diameter d_p, μ
1	Poppy seeds	1.10	1000
2	Microthene	0.64	300
3	Lucite	1.60	50

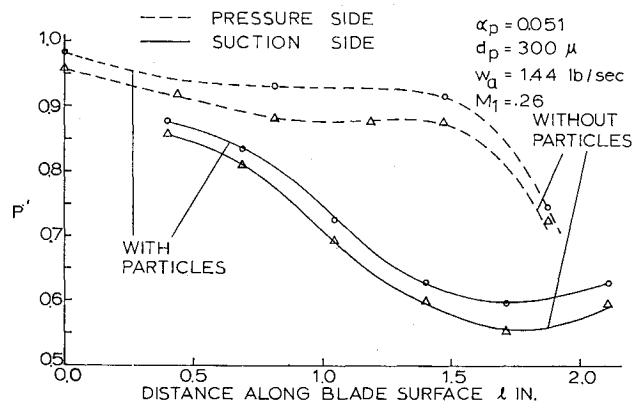

Fig. 7 Nondimensional pressure distribution on blade.

Test Results and Discussion

The experimental data show that the pressure distribution on the blade suction and pressure sides is affected by the presence of solid particles. Figures 4 and 5 show the pressure distribution on the blade for the cases with and without particles. These two figures represent a constant mean particle diameter $d_p = 50\ \mu$ and for a constant particle concentration α. The air mass flows are $W_a = 0.771$ and 1.45 lb/sec, correspondingly.

It can be observed that the pressure distributions for flows with particles are increased by a small amount with respect to those corresponding to the particle free case. A comparison of Figs. 4 and 5 indicates that the nondimensional pressure distribution over the blades will rise with a corresponding increase in Mach number or mass flow rate. This effect is intensified as the Mach number increases. This is a consequence of the rise in the level of turbulence, hence, an increase in pressure. Figures 6 and 7 show the same general trend for the case of $d_p = 300\ \mu$.

The pressure difference between flows with and without particles remains nearly constant despite the decrease in the concentration factor α and rise in the Mach number. It may be concluded from these observations that the deviation in pressure distribution is larger for a higher level of the concentration α. This increase in α will result in a drop in gas momentum and more particle collisions. This is made apparent by a rise in the pressure distribution.

The effect of a change in the particle material density $\bar{\rho}_p$ for different particle diameters d_p is difficult to assess. The reason for this is that it is necessary to use either the same particle material but different diameters, or vice versa. These requirements are difficult to meet because of the lack of a commercial source for such particles. However, in order to have some idea of the effect of changing d_p and $\bar{\rho}_p$, a comparison can be made between Figs. 5 and 7. These data are for the same concentration factor α, but with a sixfold increase in d_p from 50 to 300 μ accompanied by a one-third drop in $\bar{\rho}_p$ from 1.60 to 0.64 g/cm^3. It will be observed that there is a slightly higher pressure rise in Fig. 7. This results from the increased particle inertia because of the larger particle diameters.

Conclusion

The measurements show that the particle sizes and concentrations change the pressure distribution along the cascades and, consequently, effect the basic performance of the turbine or compressor.

Reference

[1] Tabakoff, W. and Hussein, M., "An Experimental Study of the Effect of Solid Particles on the Pressure at Blade Surface in Cascade," Project Themis Rept. 70-8, University of Cincinnati, Cincinnati, Ohio, March 1970; also U.S. Government Research and Development Rept. AD-703896.

A Correction for Compressible Subsonic Planar Flow

HELGE NØRSTRUD*
Lockheed-Georgia Company, Marietta, Ga.

THE Prandtl-Glauert similarity rule describes the pressure distribution on an airfoil in a compressible uniform stream of Mach number M_∞ in terms of the incompressible pressure distribution by the well-known formula

$$c_{pM_\infty} = c_{pi}/(1 - M_\infty^2)^{1/2} \tag{1}$$

where $c_{pi} = c_{pM_\infty=0}$ designates the incompressible pressure coefficient. This simple compressibility correction rule has been extensively applied in aerodynamics and is of fundamental importance in linearized flow analysis. However, its limitations for freestream Mach numbers approaching unity are evident from Eq. (1). Another deficiency in adopting the Prandtl-Glauert correction formula for high subsonic speeds is because of its one dimensionality, which again precludes a correct prediction of the pressure distribution at these speeds. The present Note is concerned with an improvement over the Prandtl-Glauert rule in the latter sense. A compressibility correction formula will be given which is essentially a relationship between local variables, but which can be understood as being able to include some global effects.

The earliest improvements to the Prandtl-Glauert compressibility rule came as a natural extension from the hodograph theory of compressible flow. The Kármán-Tsien formula[1] and the works of Ringleb[2] and Temple and Yarwood[3] are examples of this development. Garrick and Kaplan[4] subsequently gave a unified analysis of previous results and also introduced some new relations. Krahn[5] arrives at his formula by writing the incompressible velocity as the geometric mean of the compressible velocity and the stream density. This procedure, however, leads to an implicit expression for the compressible pressure coefficient. The relation given by

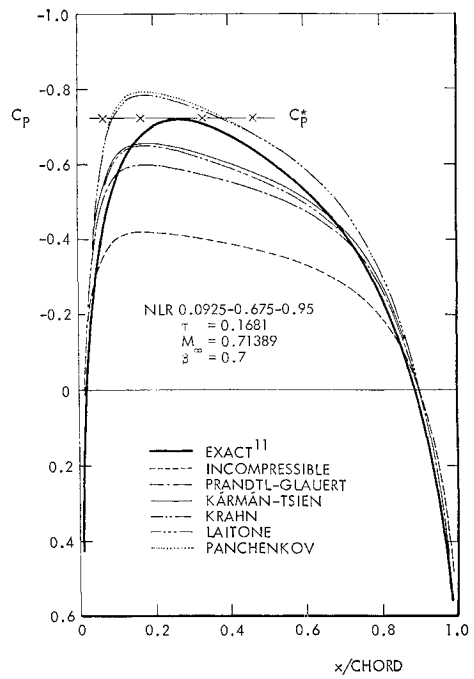

Fig. 1 Chordwise pressure distribution as obtained from various compressibility correction formulas.

Received August 17, 1970.

* Scientist, Aerospace Sciences Laboratory. Member AIAA.